Supporting Information

Fu-Ren F. Fan,[a] Juhyoun Kwak,[b] and Allen J. Bard[a*]

Department of Chemistry and Biochemistry, The University of Texas at Austin, Austin, Texas 78712 and Department of Chemistry, Korea Advanced Institute of Science and Technology, Taejon, Korea 305-701

Chronology of the Single Molecule Electrochemistry Experiments

Single molecule electrochemical detection (SMED) experiments were started on May 4, 1994. In the first experiment, we used a Pt disk (radius, 2.5 mm) as the substrate and an Apiezon-wax-coated Pt-Ir tip as the ultramicroelectrode. The tip was prepared as described in the Experimental Section, and the solution used was 2 mM Cp_2FeTMA^+ and 2 M $NaNO_3$. Two sets of cyclic voltammograms (CV) were recorded at five different tip-substrate spacings. Some hysteresis was always found in the CV when the tip was very close to the substrate. Between these two sets of CV experiments, we carried out three SECM approach (i_T vs d) experiments One of the i_T vs d curves is shown in Figure S8. There were significant differences (~50% change) in the $i_{T,\infty}$ of the two sets of CV experiments, indicating that the effective radius and geometry of the tip had changed when the tip was lowered into the tunneling region. This demonstrated that repeated approach curve experiments with a given tip geometry were not possible.

This experiment was repeated (from May 6 to May 23, 1994) with six freshly-prepared tips. Two out of six tips showed normal steady-state CVs with $i_{T,\infty}$ equal to a few picoamps in a solution containing 2 mM $CpFeTMA^+$ and 2 M $NaNO_3$. The other four were either too big or failed to show well-behaved CVs and were discarded. As with tip preparation for STM, there is some variability in tips prepared by the same procedure. In this case, variations in the conditions under which the tip end was opened (a controlled crash) led to differences in the radius of the exposed Pt-Ir and geometry of the tip end. On May 10, 1994, we used one of the two good tips to carry out an i_T vs time experiment at different tip-substrate spacings. Two of the i_T vs time curves are shown in Figure S9. Thus, the successful rate of good tip preparation is not high (~1 out of 4), and the overall experiment is very time-consuming. It took ~2 days for the preparation and characterization of one good tip and the performance of the desired experiments.

From May 27 to November 16, 1994, we used indium tin oxide (ITO) as the substrate in an SMED experiment with polyethylene-coated Pt-Ir tips. The polyethylene-coated tip was easier to prepare and was more stable than the Apiezon-wax-coated one. During this period, we focused on an investigation of the fluctuation of the tip current with various redox couples at different concentrations. We collected a number of i_T vs time curves. Some of them have been published previously with or without PDF analysis; others remain in the form of raw data. From February 3 to March 14, 1995, we carried out an experiment involving Ag deposition in the cavity of the SECM cell. The experiment was incomplete but the results clearly showed the trapping phenomenon of the particular SECM configuration.

Since March 16, 1995, we have carried out more SMED experiments with n-TiO_2 as the substrate. This experiment clearly demonstrated that the tip current fluctuation observed at very small tip-substrate spacing is associated with the positive feedback of the redox reaction and not just noise. We continued to collect more tip current histograms at various conditions and carried out statistical analyses on these data. In this paper, we show two sets of data (one for ITO and the other for n-TiO_2 substrates). Some of the tip current histograms and their PDF are given in the supporting information. The amount of data available is still limited because of the difficult and time-consuming experiments and data analysis. However, the results presented in the paper and in the supporting information are consistent.

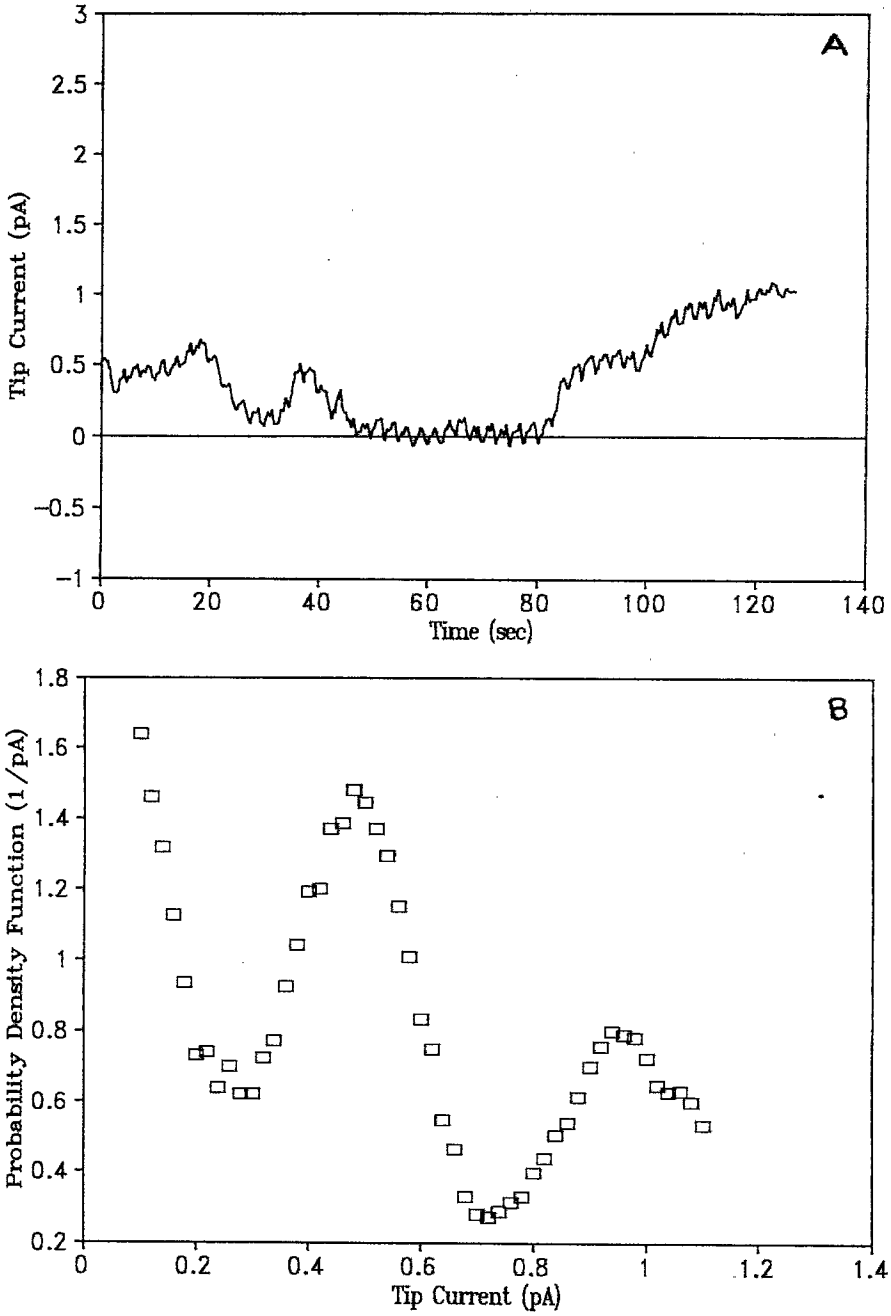

Figure S1. (A) Time histogram of the tip current observed at $E_T = 0.55$ V and an ITO substrate potential of $E_S = -0.3$ V vs SCE. $a \approx 7$ nm, $d \approx 10$ nm, solution: 2 mM Cp_2FeTMA^+ and 2.0 M $NaNO_3$. The data sampling rate was 0.4 s per point. (B) PDF of the time series in A.

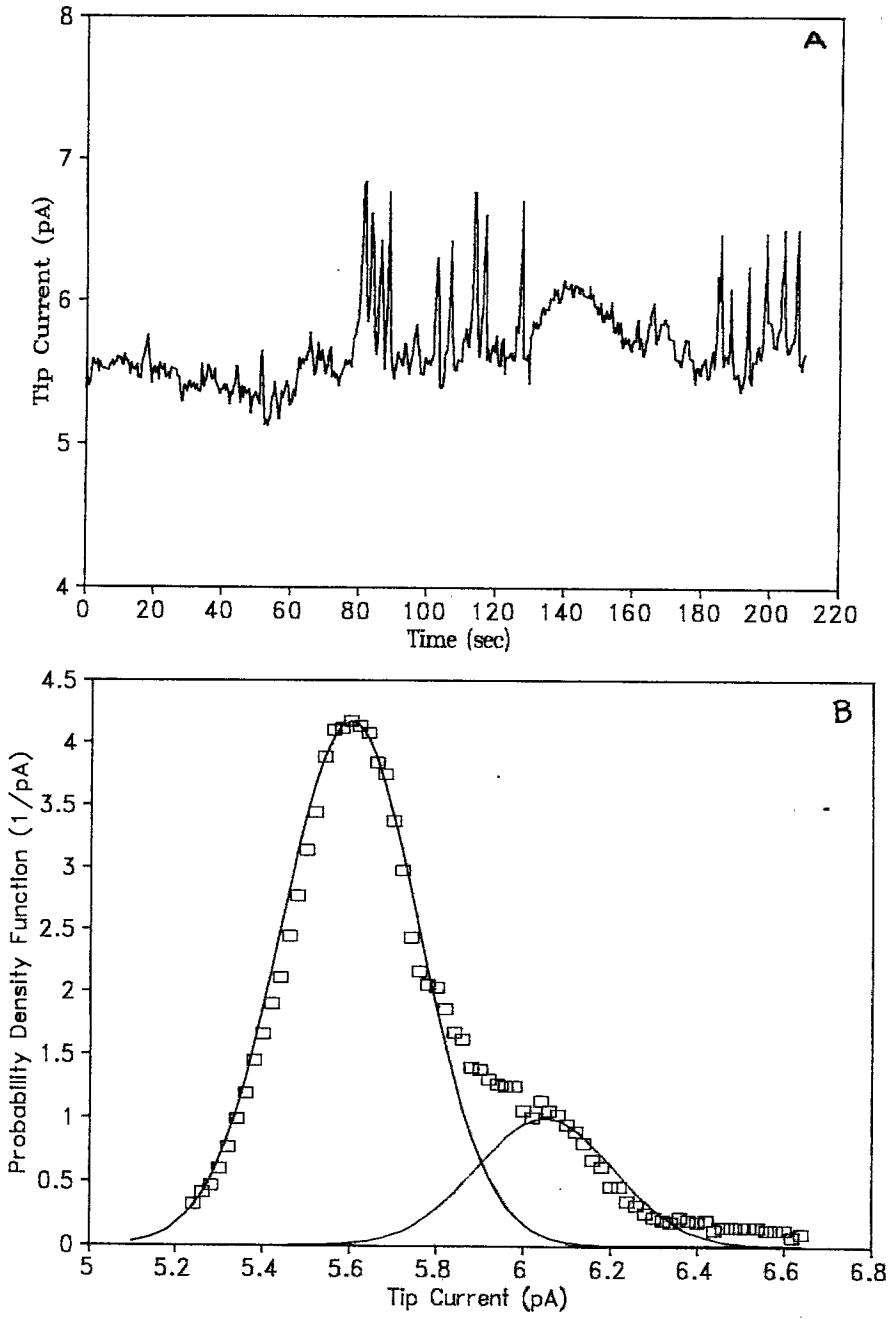

Figure S2. (A) Time evolution of the tip current observed at $E_T = 0.6$ V and an n-TiO_2 substrate potential of $E_S = -0.7$ V vs SCE. $a \approx 45$ nm, $d \approx 11$ nm, solution: 2 mM Cp_2FeTMA^+ and 1.0 M $NaNO_3$. (B) PDF of the time series in A.

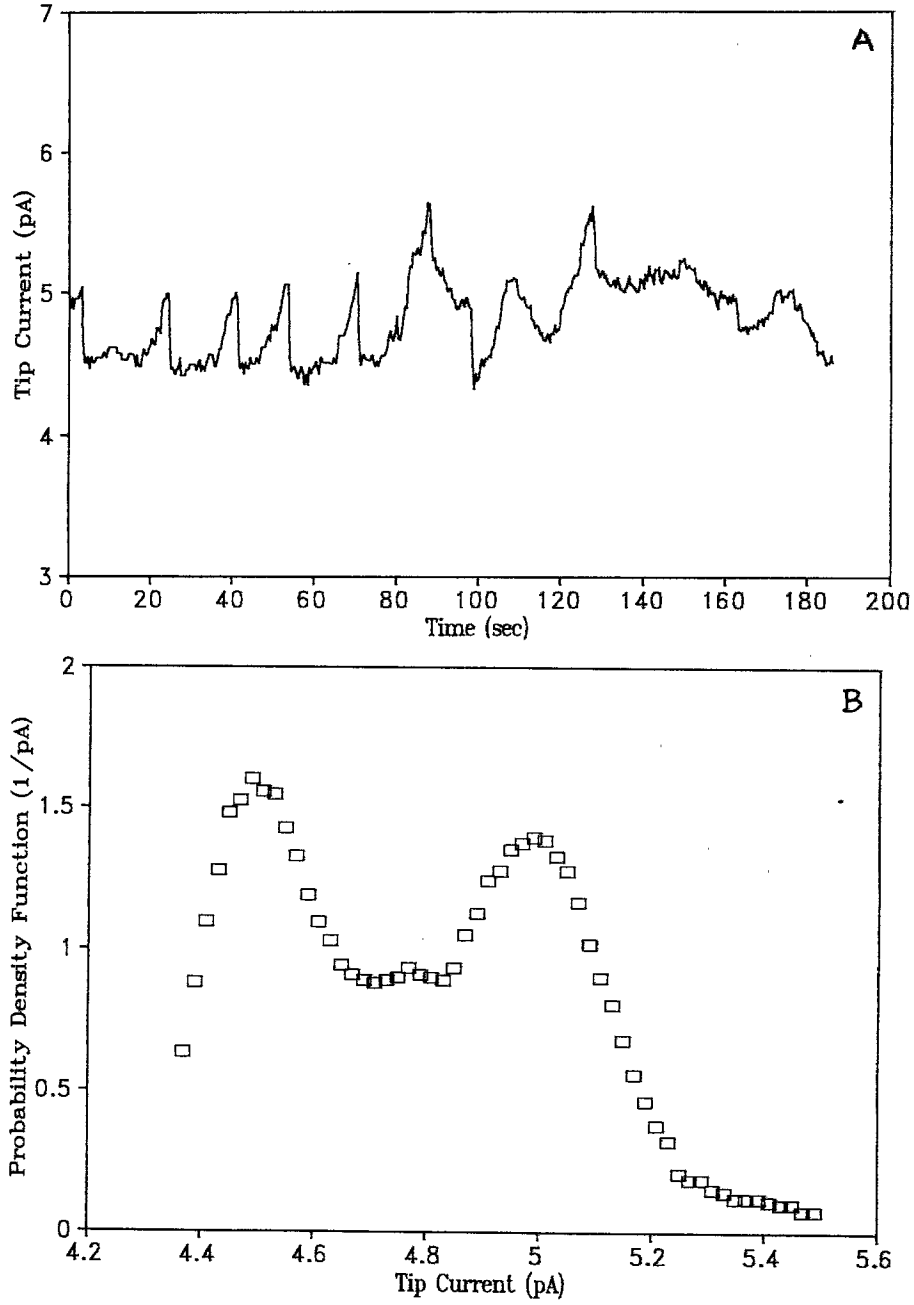

Figure S3. Another time histogram of the tip current under similar conditions as in Figure S2.

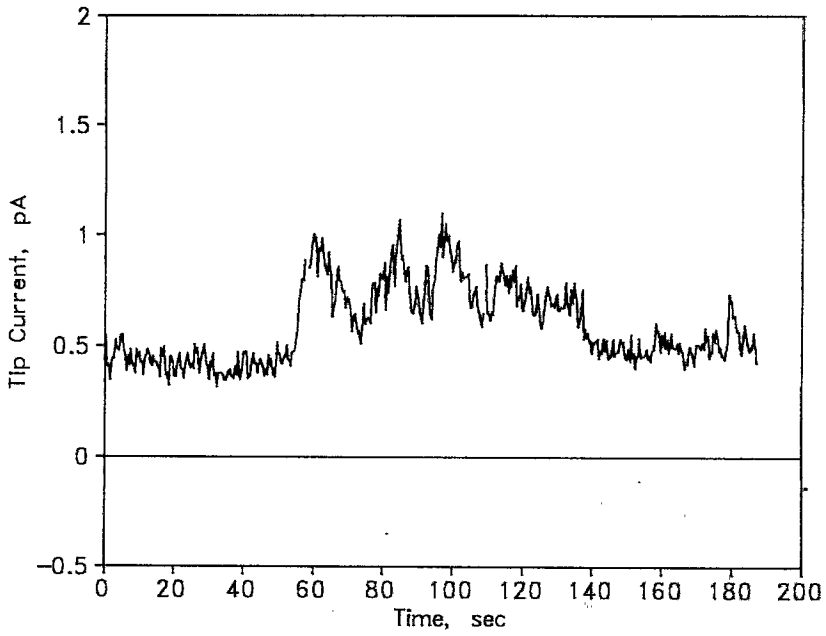

Figure S4. Time histogram of the tip current observed at $E_T = 0.5$ V and an ITO substrate potential of $E_S = -0.3$ V vs SCE. Solution: 2 mM Cp_2FeCOO^- and 0.5 M $NaNO_3$. The initial tip current was set at 0.5 pA by adjusting *d*.

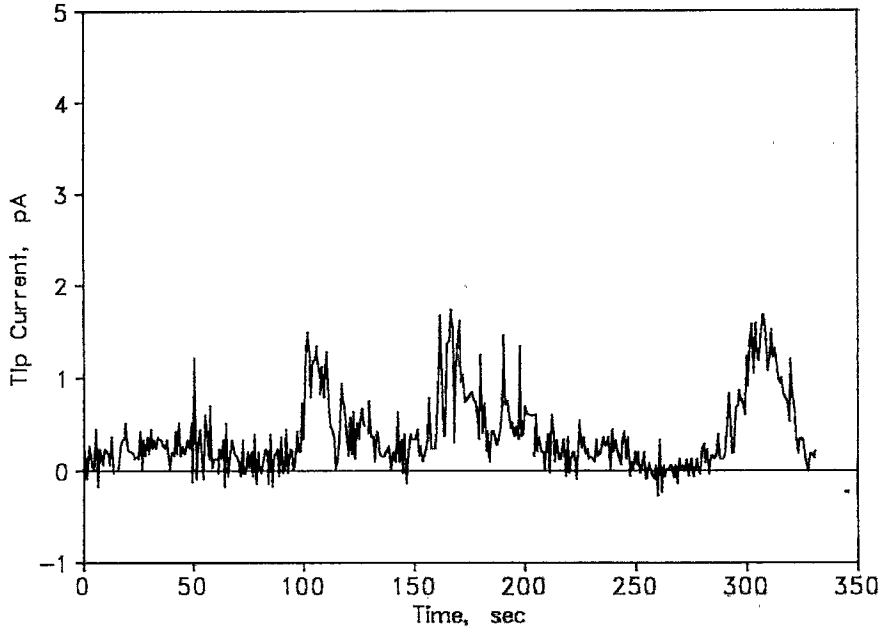

Figure S5. Time histogram of the tip current under similar conditions as in Figure S1, but with a different tip.

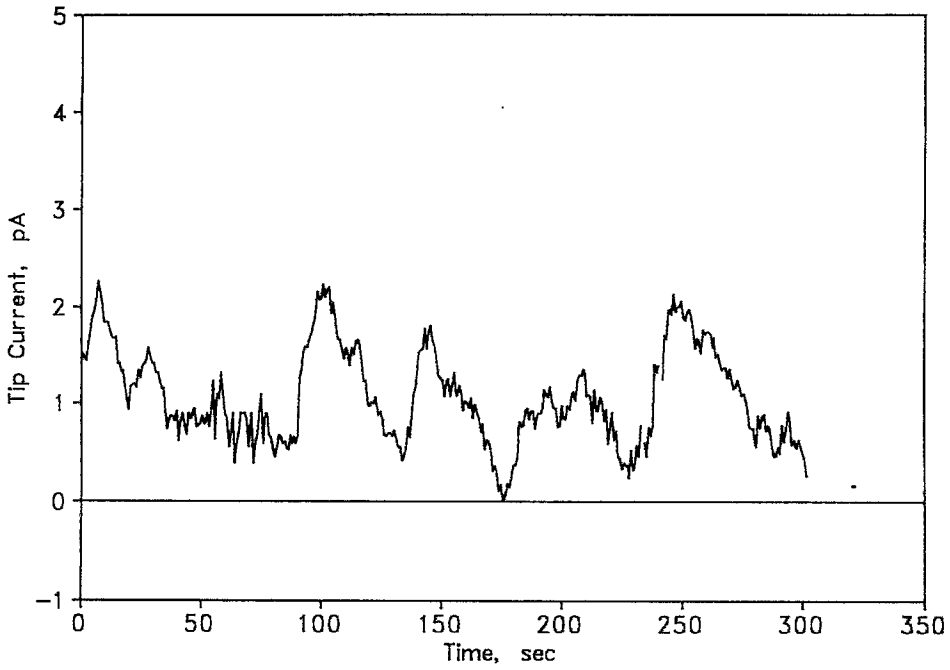

Figure S6. Time histogram of the tip current under similar conditions as in Figure S1, but with a tip different from either of those used in Figures S1 and S5.

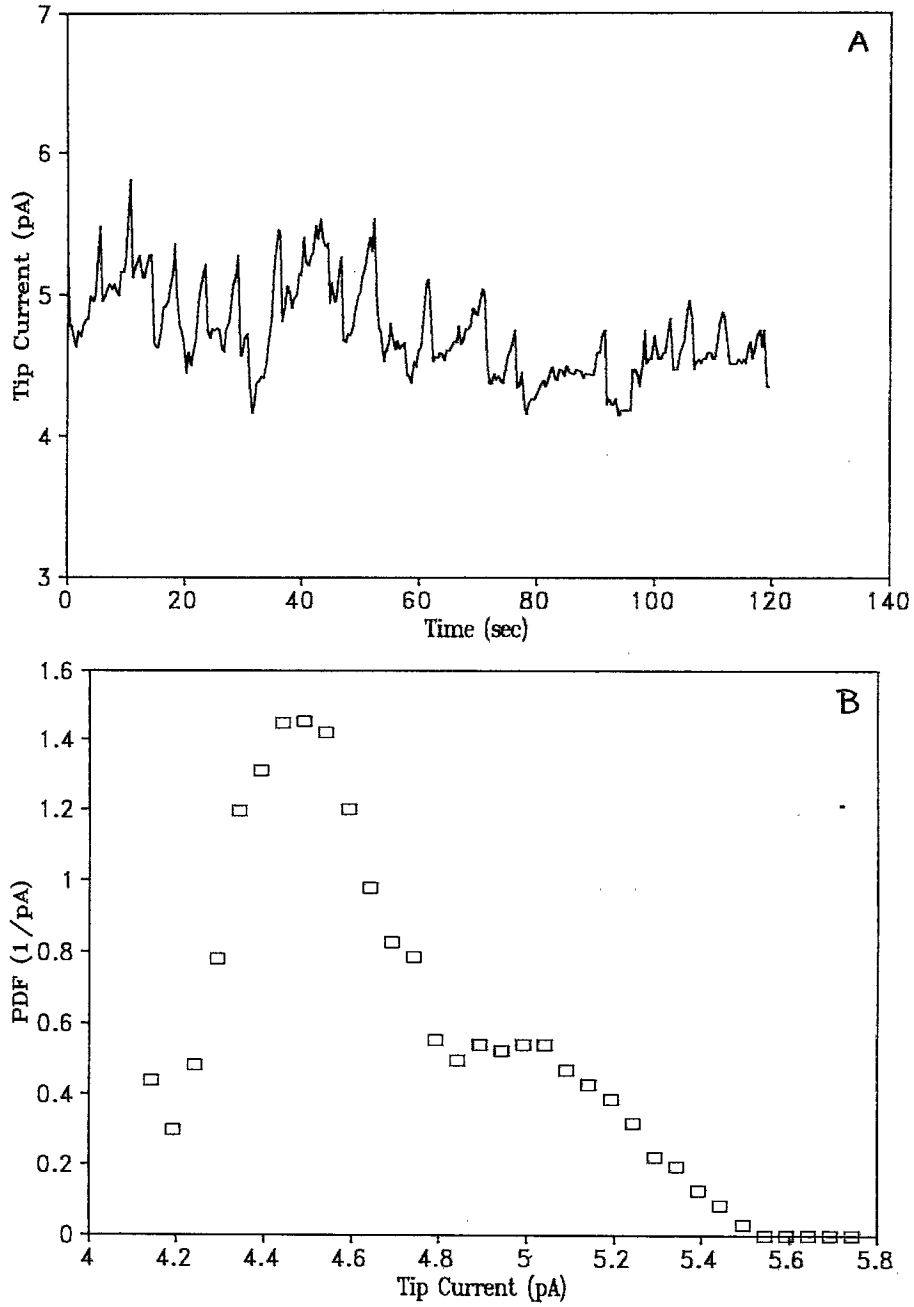

Figure S7. (A) Time histogram of the tip current under similar conditions as in Figure S2, but with a different tip. (B) PDF of the time series in A.

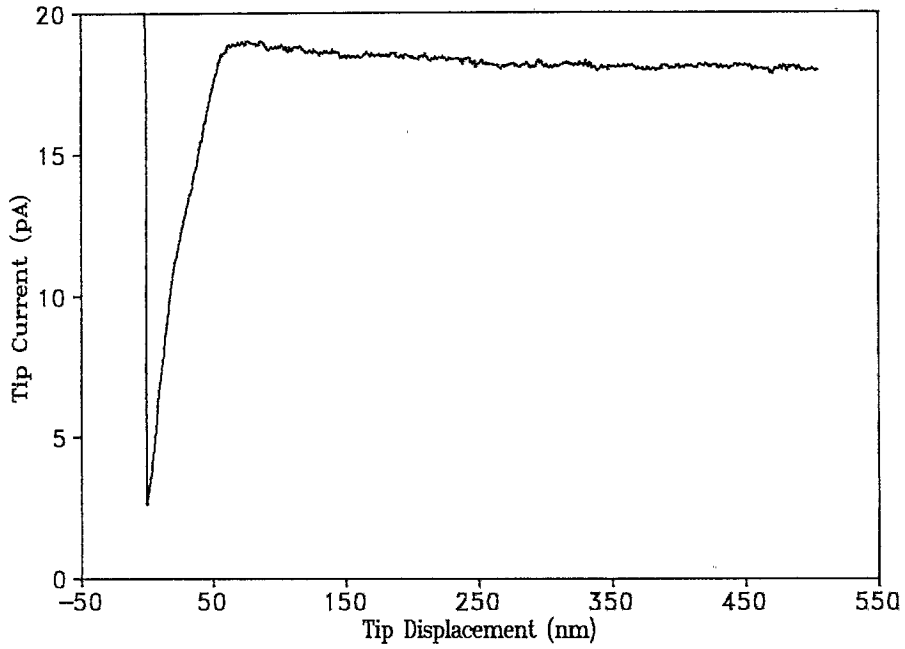

Figure S8. One of the i_T vs d curves over a Pt-disk substrate ($E_S = 0.15$ V vs SCE) in a solution containing 2 mM Cp_2FeTMA^+ and 2 M $NaNO_3$. The tip was biased at 0.60 V vs SCE.

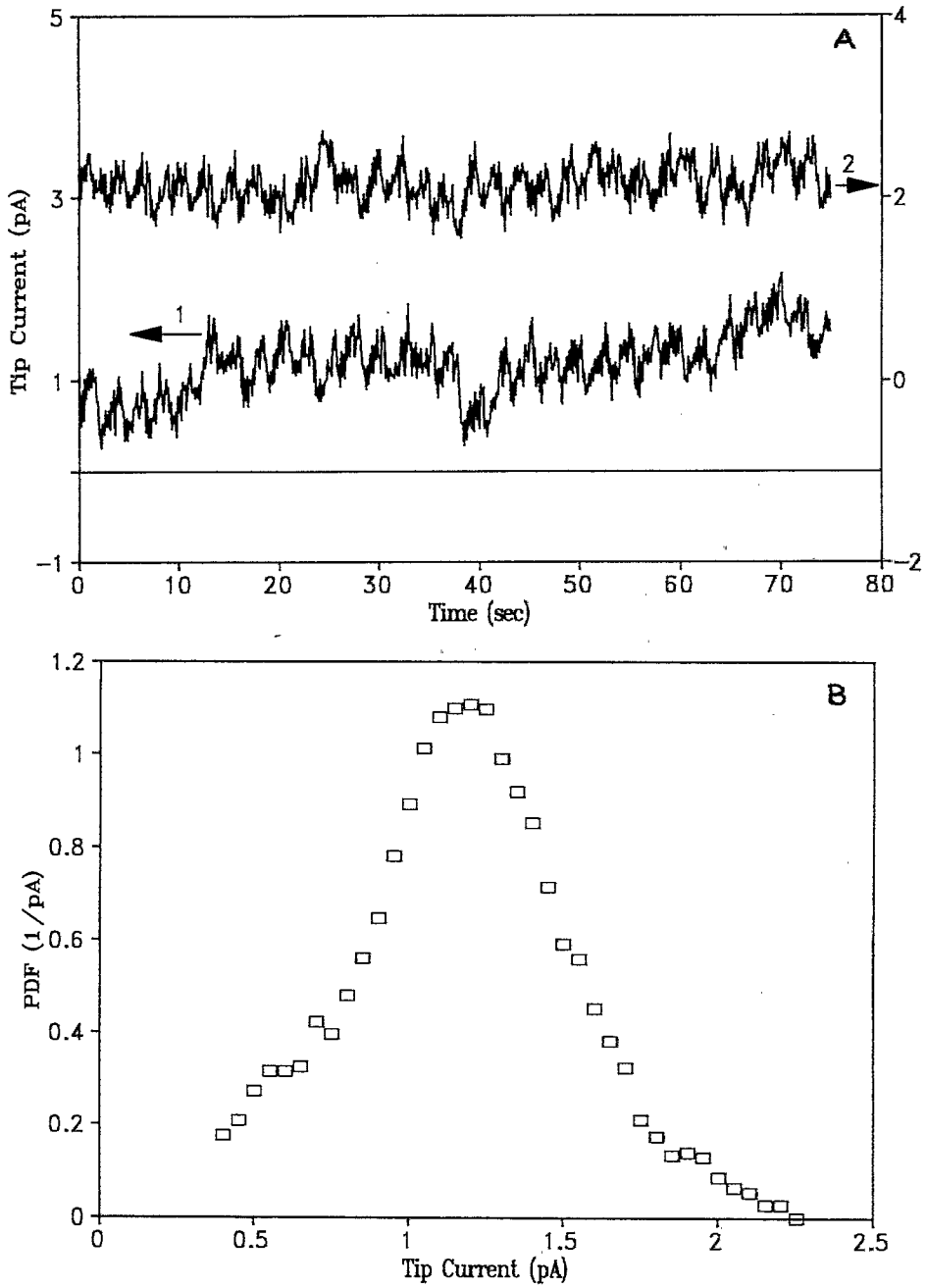

Figure S9. (A) Time evolution of the tip current observed at $E_T = 0.6$ V and a Pt disk substrate potential of $E_S = 0.11$ V vs SCE in a solution of 2 mM Cp_2FeTMA^+ and 2 M $NaNO_3$ for two different tip-substrate spacings, d. Curve 1 was at a d that gave an initial $i_T \approx 0.6$ pA, and curve 2 was at a d ~35 nm farther away from that in curve 1. (B) PDF of the time series in A, curve 1.

Digital Simulation of Current at a Recessed Tip Approaching a Conductive Substrate.

Let us consider the general diffusion problem in the axisymmetric coordinates. In the continuum mechanics, the diffusion equation of species i is described as following equation.

$$\frac{\partial C_i(r,z,t)}{\partial t} = D_i\frac{\partial^2 C_i(r,z,t)}{\partial r^2} + D_i\frac{1}{r}\frac{\partial C_i(r,z,t)}{\partial r} + \frac{\partial^2 C_i(r,z,t)}{\partial z^2} \qquad \text{(Eq.1)}$$

Instead of solving the above equation, we generally use the digitized methods(finite difference method and finite element method) to get the approximate dynamic or steady-state current response at the axisymmetric tip electrode because even the simplest problem of scanning electrochemical microscopy using a ideal disk tip electrode cannot be analytically solved yet. In this study, we employ the finite difference method algorithm for digital simulation of axisymmetric coordinates. The basic algorithm is briefly described below.

First of all, let us consider the change of number of species i in the finite volume $\delta V_{j,l}$ during the time interval between t_k and t_{k+1} for $i=1,2,\ldots,imax$, $j=0,1,\ldots,jmax$, $l=0,1,\ldots,lmax$, and $k=0,1,\ldots,kmax$.

$$N_{i,j,l,k+1} - N_{i,j,l,k} = C_{i,j,l,k+1}\cdot\delta V_{j,l} - C_{i,j,l,k}\cdot\delta V_{j,l} \qquad \text{(Eq.2).}$$

or by mass conservation law in $\delta V_{j,l}$ which results in the Fick's second law

$$\begin{aligned} N_{i,j,l,k+1} - N_{i,j,l,k} = \; & J_{i,j,l/l+1,k/k+1}\; A_{j,l/l+1}\; \Delta t_k \\ & -J_{i,j+1,l/l+1,k/k+1}\; A_{j+1,l/l+1}\; \Delta t_k \\ & +J_{i,j/j+1,l,k/k+1}\; A_{j/j+1,l}\; \Delta t_k \\ & -J_{i,j/j+1,l+1,k/k+1}\; A_{j/j+1,l+1}\; \Delta t_k \end{aligned} \qquad \text{(Eq.3)}$$

where

$\delta V_{j,l}$ is the volume in the range of $r_j \le r \le r_{j+1}$ and $z_l \le z \le z_{l+1}$,

$N_{i,j,l,k}$ is the number of species i in $\delta V_{j,l}$ at t_k,

$C_{i,j,l,k}$ is the average concentration of species i in $\delta V_{j,l}$ at t_k,

$\Delta t_k = t_{k+1} - t_k$,

$A_{j,l/l+1}$ is the surface at r_j in the range of $z_l \le z \le z_{l+1}$,

$J_{i,j,l/l+1,k/k+1}$ is the average flux of species i at $A_{j,l/l+1}$ between t_k and t_{k+1},

$A_{j/j+1,l}$ is the surface at z_l in the range of $r_j \le r \le r_{j+1}$,

and $J_{i,j/j+1,l,k/k+1}$ is the average flux of species i at $A_{j/j+1,l}$ between t_k and t_{k+1}.

From (Eq.2) and (Eq.3),

$$\begin{aligned} C_{i,j,l,k+1}\cdot\delta V_{j,l} - C_{i,j,l,k}\cdot\delta V_{j,l} = \; & J_{i,j,l/l+1,k/k+1}\; A_{j,l/l+1}\; \Delta t_k \\ & -J_{i,j+1,l/l+1,k/k+1}\; A_{j+1,l/l+1}\; \Delta t_k \\ & +J_{i,j/j+1,l,k/k+1}\; A_{j/j+1,l}\; \Delta t_k \\ & -J_{i,j/j+1,l+1,k/k+1}\; A_{j/j+1,l+1}\; \Delta t_k \end{aligned} \qquad \text{(Eq.4).}$$

Flux of species i at a surface can be approximated by the Fick's first law. But there are fundamentally two ways of approximation to obtain the average flux of species i between t_k and t_{k+1}. For example, at $A_{j,l/l+1}$,

$$J_{i,j,l/l+1,k/k+1} \approx J_{i,j,l/l+1,k} = -D_i\left(\frac{C_{i,j,l,k} - C_{i,j-1,l,k}}{r_j - r_{j-1}}\right) \qquad \text{(Eq.5)}$$

or

$$J_{i,j,l/l+1,k/k+1} \approx J_{i,j,l/l+1,k+1} = -D_i\left(\frac{C_{i,j,l,k+1} - C_{i,j-1,l,k+1}}{r_j - r_{j-1}}\right) \qquad \text{(Eq.6).}$$

The former approximation method is called as the explicit method, while the latter the implicit method. There are couple of variations. For example, the Crank-Nicholson method uses the following approximation.

$$\begin{aligned} J_{i,j,l/l+1,k/k+1} &\approx \frac{J_{i,j,l/l+1,k} + J_{i,j,l/l+1,k+1}}{2} \\ &= -\frac{1}{2}D_i\left(\frac{C_{i,j,l,k} - C_{i,j-1,l,k}}{r_j - r_{j-1}}\right) - \frac{1}{2}D_i\left(\frac{C_{i,j,l,k+1} - C_{i,j-1,l,k+1}}{r_j - r_{j-1}}\right) \end{aligned} \qquad \text{(Eq.7).}$$

The above formulations can be used to solve the diffusion problems in any geometry.

This algorithm can be inductively justified with ease for the planar and axisymmetric diffusion as discussed below. For example, (Eq.4) is reduced to the well-known planar diffusion equation[1,2] with the linear space and time gridding in the rectangular coordinates by the explicit approximation method.

$$\begin{aligned}(C_{i,j,k+1}-C_{i,j,k})A\Delta x &\approx J_{i,j,k}A\,\Delta t - J_{i,j+1,k}A\,\Delta t \\ \frac{C_{i,j,k+1}-C_{i,j,k}}{\Delta t} &\approx \frac{J_{i,j,k}-J_{i,j+1,k}}{\Delta x} \\ &= \frac{-D_i\left(\frac{C_{i,j,k}-C_{i,j-1,k}}{\Delta x}\right)+D_i\left(\frac{C_{i,j+1,k}-C_{i,j,k}}{\Delta x}\right)}{\Delta x} \\ &= \frac{D_i\left(\frac{C_{i,j+1,k}-C_{i,j,k}}{\Delta x}\right)-D_i\left(\frac{C_{i,j,k}-C_{i,j-1,k}}{\Delta x}\right)}{\Delta x}\end{aligned} \qquad \text{(Eq.8)}$$

since $A = A_j = A_{j,l/l+1} = A_{j+1,l/l+1}$ and $\delta V = \delta V_{j,l} = A\Delta x$.

As $\Delta t \to 0$ and $\Delta x \to 0$, $\frac{\partial C_i}{\partial t} = \frac{\partial}{\partial x}\left(D_i\frac{\partial C_i}{\partial x}\right)$ or $\frac{\partial C_i}{\partial t} = D_i\frac{\partial^2 C_i}{\partial x^2}$. (Eq.9)

Likewise, (Eq.4) is reduced to (Eq.1) with the linear space and time gridding in the axisymmetric coordinates by the explicit approximation method.

$$\begin{aligned}\frac{(C_{i,j,l,k+1}-C_{i,j,l,k})}{\Delta t} \approx\ & J_{i,j,l/l+1,k}\ \frac{2\pi r_j\Delta z}{\pi(r_{j+1}^2-r_j^2)\Delta z} \\ & -J_{i,j+1,l/l+1,k}\ \frac{2\pi r_{j+1}\Delta z}{\pi(r_{j+1}^2-r_j^2)\Delta z} \\ & +J_{i,j/j+1,l,k}\ \frac{\pi(r_{j+1}^2-r_j^2)}{\pi(r_{j+1}^2-r_j^2)\Delta z} \\ & -J_{i,j/j+1,l+1,k}\ \frac{\pi(r_{j+1}^2-r_j^2)}{\pi(r_{j+1}^2-r_j^2)\Delta z} \\ =\ & J_{i,j,l/l+1,k}\ \frac{2r_j}{(r_{j+1}+r_j)(r_{j+1}-r_j)} \\ & -J_{i,j+1,l/l+1,k}\ \frac{2r_{j+1}}{(r_{j+1}+r_j)(r_{j+1}-r_j)} \\ & +J_{i,j/j+1,l,k}\ \frac{1}{\Delta z} \\ & -J_{i,j/j+1,l+1,k}\ \frac{1}{\Delta z}\end{aligned} \qquad \text{(Eq.10)}$$

$$\begin{aligned}&\frac{(C_{i,j,l,k+1}-C_{i,j,l,k})}{\Delta t} \approx \\ &\frac{1}{(r_{j+1}+r_j)/2}\left\{\frac{D_i r_{j+1}\left(\frac{C_{i,j+1,l,k}-C_{i,j,l,k}}{\Delta r}\right)-D_i r_j\left(C_{i,j,l,k}-\frac{C_{i,j-1,l,k}}{\Delta r}\right)}{\Delta r}\right\} \\ &+\frac{D_i\left(\frac{C_{i,j,l+1,k}-C_{i,j,l,k}}{\Delta z}\right)-D_i\left(\frac{C_{i,j,l,k}-C_{i,j,l-1,k}}{\Delta z}\right)}{\Delta z}\end{aligned} \qquad \text{(Eq.11)}$$

since $A_{j,l/l+1} = 2\pi r_j\Delta z$, $A_{j+1,l/l+1} = 2\pi r_{j+1}\Delta z$,
$A_{j/j+1,l} = A_{j/j+1,l+1} = \pi(r_{j+1}^2-r_j^2)$, and $\delta V_{j,l} = \pi(r_{j+1}^2-r_j^2)\Delta z$.
As $\Delta t \to 0$, $\Delta r \to 0$, and $\Delta z \to 0$,

$$\frac{\partial C_i}{\partial t} = \frac{1}{r}\frac{\partial}{\partial r}\left(D_i r \frac{\partial C_i}{\partial r}\right) + \frac{\partial}{\partial z}\left(D_i \frac{\partial C_i}{\partial z}\right)$$
$$= D_i \frac{1}{r}\frac{\partial}{\partial r}\left(r \frac{\partial C_i}{\partial r}\right) + D_i \frac{\partial}{\partial z}\left(\frac{\partial C_i}{\partial z}\right) \qquad \text{(Eq.12)}$$
$$= D_i \frac{\partial^2 C_i}{\partial r^2} + D_i \frac{1}{r}\frac{\partial C_i}{\partial r} + D_i \frac{\partial^2 C_i}{\partial z^2}$$

Obviously, the accuracy of digital simulation will be increased with greater number of grids with small time and space steps of $\Delta t \rightarrow 0$, $\Delta r \rightarrow 0$, and $\Delta z \rightarrow 0$. Exponentially expanding time and space gridding method is generally used to reduce the burden of computing time with small $kmax$, $jmax$, and $lmax$ integer values. Also, generally the finer grid is adapted in the region of the stiff concentration variation, for example near the electrodes.

For the approximate simulation of diffusion with the axisymmetric recessed tip electrode, the simplified geometry as shown below is adapted. The gap between the tip electrode and substrate is defined as d. The radius of tip electrode is a. The distance from the center to the outer layer of insulating sheath is defined as R_{glass}. The recessed distance of disk electrode is $z_{recess} < d$. In this simplified geometry, there are zones of no interest. Apparently, there is no diffusion in the zone of insulating sheath as well as the fluxes at the boundary surfaces of this zone are zero. For the simplicity, it is assumed that the concentrations in the zone of bulk solution are approximated as the bulk concentrations throughout all the time. This simplified assumption can be fulfilled by an imaginary electrode(dotted line) of very positive potential, i.e. $E_{imag} \gg E^o_{Red/Ox}$. although there is no real boundary between the zones of trapped solution and bulk solution, It is needless to say that the fluxes through the boundary surface at the symmetric axis are zero.

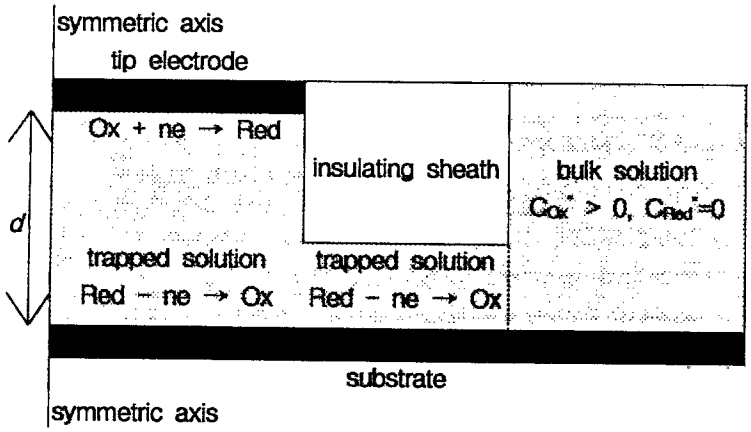

In result, the diffusion region to be solved is confined to the region of the trapped solution as shown above with an imaginary boundary surface. The fluxes at the tip electrode and conductive substrate electrode can be calculated by Butler-Volmer[1,3] model with $E_{tip} \ll E^o_{Red/Ox}$, $k^o_{tip} \rightarrow \infty$ and $E_{substrate} \gg E^o_{Red/Ox}$, $k^o_{substrate} \rightarrow \infty$.

Indexing of space grid starts from substrate and symmetric axis,

i.e. $r_0, r_1, r_2, \ldots, r_{ig-1}, r_{ig}, r_{ig+1}, \ldots, r_j, \ldots, r_{jmax}$ in r direction

and $z_0, z_1, z_2, \ldots, z_{lg-1}, z_{lg}, z_{lg+1}, \ldots, z_l, \ldots, z_{lmax}$ in z direction

where $r_0 = 0$, $z_0 = 0$, $r_{ig} = R_{glass} - a$, and $z_{lg} = d - z_{recess}$.

Exponentially expanding space gridding method[4,5] is used for the efficient gridding with small $jmax$ and $lmax$ integer values. Also, generally the finer grid is adapted in the region of the stiff concentration variation, for example near the electrodes. The finest grids in r direction should starts at the edge of tip electrode($r = a$) and as well as at the imaginary electrode($r = R_{glass}$). The finest grids in z direction should starts on

both side of tip and substrate electrodes($z=0$ and $z=d$) as well as near $z_{lg}=d-z_{recess}$ where there is the boundary of insulating sheath. In the simulation, $jmax=24$, $lmax=24$, $jg=10$, and $lg=12$ with $\Delta r=\Delta z=0.01a$. Three different sections of exponentially expanding space gridding are needed in the r direction, i.e. 1st section, $r_j-r_{j-1}=\Delta r_j=\exp(\beta_{r1}^{10-j})\Delta r$ for $j=1,2,\ldots,10$ where $r_{10}=a$ and $r_0=0$; 2nd section, $r_j-r_{j-1}=\Delta r_j=\exp(\beta_{r2}^{j-11})\Delta r$ for $j=11,12,\ldots,17$ where $r_{10}=a$ and $r_{17}=a+(R_{glass}-a)/2$; 3rd section, $r_j-r_{j-1}=\Delta r_j=\exp(\beta_{r3}^{24-j})\Delta r$ for $j=18,19,\ldots,24$ where $r_{24}=R_{glass}$ and $r_{17}=a+(R_{glass}-a)/2$. In the z direction, four different sections of exponentially expanding space gridding are needed, i.e. 1st section, $z_l-z_{l-1}=\Delta z_l=\exp(\beta_{z1}^{l-1})\Delta z$ for $z=1,2,\ldots,6$ where $z_0=0$ and $z_6=(d-z_{recess})/2$; 2nd section, $z_l-z_{l-1}=\Delta z_l=\exp(\beta_{z2}^{12-l})\Delta z$ for $z=7,8,\ldots,12$ where $z_{12}=(d-z_{recess})$ and $z_6=(d-z_{recess})/2$; 3rd section, $z_l-z_{l-1}=\Delta z_l=\exp(\beta_{z3}^{l-13})\Delta z$ for $z=13,14,\ldots,18$ where $z_{12}=(d-z_{recess})$ and $z_{18}=d-z_{recess}/2$; 4th section, $z_l-z_{l-1}=\Delta z_l=\exp(\beta_{z4}^{24-l})\Delta z$ for $z=19,20,\ldots,24$ where $z_{24}=d$ and $z_6=(d-z_{recess})/2$. Once r_j and z_l for $j=0,1,\ldots,jmax$ and $l=0,1,\ldots,lmax$ are defined, the calculations of $A_{j,l/l+1}$, $A_{j/j+1,l}$ and $\delta V_{j,l}$ are straightforward, i.e. $A_{j,l/l+1}=2\pi r_j(z_{l+1}-z_l)$, $A_{j/j+1,l}=\pi(r_{j+1}^2-r_j^2)$, and $\delta V_{j,l}=\pi(r_{j+1}^2-r_j^2)(z_{l+1}-z_l)$.

The remained one is a matter of calculation with the appropriate small space and time steps. In general, since the explicit method is practically unstable in the time marching of large time steps, the stable implicit method is usually employed to solve the diffusion problem. The one dimensional diffusion problem can be solved by rather simple inversion of a band matrix. In two dimensional diffusion problem, the matrix is too huge to inverse. One of the technique to overcome this calculation problem is the ADI(alternate-direction implicit) method[6]. ADI method is based on the time splitting on the physical phenomena. Even though the fluxes at the surfaces of the finite volume $\delta V_{j,l}$ during the time interval between t_k and t_{k+1} are physically occurred at the same time, in the ADI method, it is assumed that the two-kind of fluxes at the surfaces are occurred during two different half-steps of time. For example, in the axisymmetric coordinates, the fluxes in r and z direction is approximated as explicit and implicit during t_k and $t_{k+1/2}$ while the fluxes in r and z direction is approximated as implicit and explicit during $t_{k+1/2}$ and t_{k+1} where $t_{k+1/2}=\frac{t_k+t_{k+1}}{2}$. Therefore, (Eq.4) can be further approximated by two-splitted operating steps,

$$\begin{aligned} C_{i,j,l,k+1/2}\cdot\delta V_{j,l}-C_{i,j,l,k}\cdot\delta V_{j,l}\approx\ & J_{i,j,l/l+1,k}\quad A_{j,l/l+1}\quad(\Delta t_k/2)\\ & -J_{i,j+1,l/l+1,k}\quad A_{j+1,l/l+1}\quad(\Delta t_k/2)\\ & +J_{i,j/j+1,l,k+1/2}\quad A_{j/j+1,l}\quad(\Delta t_k/2)\\ & -J_{i,j/j+1,l+1,k+1/2}\quad A_{j/j+1,l+1}\quad(\Delta t_k/2) \end{aligned} \qquad \text{(Eq.13)}$$

and

$$\begin{aligned} C_{i,j,l,k+1}\cdot\delta V_{j,l}-C_{i,j,l,k+1/2}\cdot\delta V_{j,l}\approx\ & J_{i,j,l/l+1,k+1}\quad A_{j,l/l+1}\quad(\Delta t_k/2)\\ & -J_{i,j+1,l/l+1,k+1}\quad A_{j+1,l/l+1}\quad(\Delta t_k/2)\\ & +J_{i,j/j+1,l,k+1/2}\quad A_{j/j+1,l}\quad(\Delta t_k/2)\\ & -J_{i,j/j+1,l+1,k+1/2}\quad A_{j/j+1,l+1}\quad(\Delta t_k/2) \end{aligned} \qquad \text{(Eq.14).}$$

Considering (Eq.13) for the specific j, it is easy to calculate the first and second terms of the right side of (Eq.13) by (Eq.5) because these are explicit form, while it becomes a matrix inversion problem for the third and fourth terms.

$$
\begin{aligned}
C_{i,j,l,k+1/2} - C_{i,j,l,k} \approx\ & -D_i\left(\frac{C_{i,j,l,k} - C_{i,j-1,l,k}}{r_j - r_{j-1}}\right) \frac{A_{j,j/l+1}\Delta t_k/2}{\delta V_{j,l}} \\
& +D_i\left(\frac{C_{i,j+1,l,k} - C_{i,j,l,k}}{r_{j+1} - r_j}\right) \frac{A_{j+1,j/l+1}\Delta t_k/2}{\delta V_{j,l}} \\
& -D_i\left(\frac{C_{i,j,l,k+1/2} - C_{i,j,l-1,k+1/2}}{z_l - z_{l-1}}\right) \frac{A_{jl/j+1,l}\Delta t_k/2}{\delta V_{j,l}} \\
& +D_i\left(\frac{C_{i,j,l+1,k+1/2} - C_{i,j,l,k+1/2}}{z_{l+1} - z_l}\right) \frac{A_{jl/j+1,l+1}\Delta t_k/2}{\delta V_{j,l}}
\end{aligned}
\qquad \text{(Eq.15)}
$$

for $l = 1, 2, \ldots, l_{max}$.

For the specific j, (Eq.15) is same as the one dimensional diffusion problem in z direction. The setup of matrix equation can be practiced in the same way as the implicit method of one dimensional diffusion equation with the coupled heterogeneous reaction. (Eq.14) also can be represented as the matrix form in the similare procedure. In result, (Eq.13) is the problem of ***jmax*** matrix inversions in the direction of z for $j = 1, 2, \ldots, j_{max}$ while (Eq.14) the problem of ***lmax*** matrix inversions in the direction of r for $l = 1, 2, \ldots, l_{max}$.

Unfortunately, the C++ object codes of the above algorithm turns out to be hardly listed in the document form because it is over 10,000 lines in total. The codes is compiled by Turbo-C++ Version 3.0 (Borland International, Inc.) in the DOS system of IBM-PC compatible with Pentium-60 CPU.

References

1. A. J. Bard and L. R. Faulkner, "Electrochemical Methods : Fundamentals and Applications", John Wiley & Sons, New York (1980), Chapter 3 and 4.
2. S. W. Feldberg in "Electroanalytical Chemistry", Vol 3, A. J. Bard, Ed., Marcel Dekker, New York (1969).
3. "Computers in Chemistry and Instrumentation," Vol 2, "Electrochemistry : Calculation, Simulation, and Instrumentation", J. S. Mattson, H. B. Mark, Jr., and H. C. MacDonald, Jr., Eds., Marcel Dekker, New York (1972).
4. S. W. Feldberg, *J. Electoranal. Chem.*, **127**, 1 (1981).
5. J. Kwak and A. J. Bard, *Anal. Chem.*, **61**, 1221 (1989).
6. W. H. Press, B. P. Flannery, S. A. Teukolsky, and W. T. Vetterling, "Numerical Recipes in C : The Art of Scientific Computing", Cambridge University Press, Cambridge (1988), pp. 681-688.